

# Heterogeneous graph neural network for power allocation in multicarrier-division duplex cell-free massive MIMO systems

Bohan Li, Lie-Liang Yang, *Fellow, IEEE*, Rob Maunder, *Senior Member, IEEE*, Songlin Sun, *Senior Member, IEEE*, Pei Xiao, *Senior Member, IEEE*

**Abstract**—In-band full duplex-based cell-free (IBFD-CF) systems suffer from severe interference problem including self-interference (SI) and cross-link interference (CLI), especially when cell-free (CF) systems are operated in a distributed way. To this end, we propose multicarrier-division duplex (MDD) as an enabler for full-duplex (FD)-style operation in distributed CF massive MIMO systems, where DL and UL transmissions take place simultaneously at the same frequency band but mutually orthogonal subcarrier sets. In order to maximize the spectral efficiency (SE) in the proposed systems, we present heterogeneous graph neural network specific for CF systems (CF-HGNN), which consists of an adaptive node embedding layer, meta-path based message passing, meta-path based attention and downstream power allocation learning. In particular, the adaptive node embedding layer can handle the varying number of access points (APs), mobile stations (MSs) and subcarriers, and the involved attention mechanism enables each AP/MS node in CF-HGNN to aggregate the information from interfering path and communication path with different priorities. Numerical results show that CF-HGNN is capable of using  $10^4$  times less operation time to achieve the 99% performance of the SE of quadratic transform and successive convex approximation (QT-SCA). Additionally, CF-HGNN also significantly outperforms unfair greedy method in terms of SE performance. Furthermore, CF-HGNN exhibits good adaptivity to varying number of nodes and subcarriers, and also generalization ability to different sizes of CF network.

**Index Terms**—multicarrier-division duplex, cell-free, massive MIMO, heterogeneous graph neural network

## I. INTRODUCTION

With the unprecedented increase of data-hungry devices, wireless communication community have been continuing to thrive in the last few years for seeking the cutting-edge techniques to further improve spectral efficiency (SE) and quality of services (QoS). In this regard,

B. Li, L.-L. Yang and R. Maunder are with the School of Electronics and Computer Science, University of Southampton, SO17 1BJ, UK. (E-mail: bl2n18, lly, rm@ecs.soton.ac.uk, <http://www-mobile.ecs.soton.ac.uk/lly>). S. Sun is with the School of Information and Communication Engineering, Beijing University of Posts and Telecommunications (BUPT). P. Xiao is with 5GIC & 6GIC, Institute for Communication Systems (ICS), University of Surrey, Guildford GU2 7XH, UK. (Email: p.xiao@surrey.ac.uk) The project was supported in part by the EPSRC, UK, under Project EP/P034284/1 and EP/P03456X/1, and in part by the Innovate UK project.

Cell-free massive MIMO (CF mMIMO) and in-band Full-duplex (IBFD) have been envisioned to be main pillars of future wireless communication systems. CF mMIMO, integrating the concept of no cell boundaries and distributed antenna mMIMO system, is capable of providing users within the coverage area with not only higher data rates but more consistent service than conventional small-cell or co-located mMIMO systems [1]. As to IBFD, it has the potential to double the SE with off-the-shelf system resource, and resolve the critical defects of traditional half-duplex (HD) modes such as inefficiency of time-frequency resource arrangement and high latency in both physical and network layers [2].

However, to date, although there have already been a large number of work on CF mMIMO [3] and IBFD systems [4], few research considers the combination of these two techniques. One of the underlying reasons is that IBFD-based CF (IBFD-CF) systems suffer from the severe self-interference (SI) and cross-link interference (CLI) problems. The SI refers to the interference that a transmitting access point (AP) causes to itself, which can be mitigated by propagation-, analog- and digital-domain SI cancellation (SIC) methods [5–9]. But the SIC implementation imposes large complexity and resource burden on small-scale APs of CF networks [10], and none of the existing methods can fully suppress the SI, leading to the performance degradation of desired transmission caused by residual SI. Furthermore, CLI, known as inter-AP interference (IAI) and inter-mobile station (MS) interference (IMI), have shown to be the most serious problem in multi-cell IBFD and dynamic TDD (DTDD) systems [11], and the situation is exacerbated in CF networks due to the dense distribution of APs, as the IAI received at each AP may come from various directions. Noticeably, compared with the IAI, the IMI is much more difficult to handle, as the baseband processors in MSs are not as powerful as those in APs. However, since the transmit power of MS is relatively small, the IMI can be largely mitigated in analog domain by power control and user scheduling [12].

### A. Related Works

In [13], authors investigated the centralized IBFD-CF systems, where collaborative zero-forcing (ZF) beamforming is applied. Although the proposed IBFD-CF largely

outperforms its HD-CF counterpart, it is hardly implementable, since IAI mitigation is heavily relied on the large path-loss, and the proposed digital-domain method can only provide very limited IAI suppression. Nevertheless, APs are usually configured at high locations, such as roof and lamps, and the path-loss of AP-AP links is not as large as that of AP-MS links or MS-MS links. In [14, 15], authors proposed a so-called network-assisted FD mode in the centralized CF networks, where digital-domain IAI and IMI are mitigated by central CPU and user scheduling, respectively, while the analog-domain interference suppression is not considered. However, in this case, the digital-domain IAI mitigation requires relatively precise IAI channel estimation as well as undistorted fronthaul transmissions, which significantly increase the system overhead. Furthermore, to our best knowledge, there is no research in open literature on FD-style distributed CF systems, as the CLI problem in distributed CF systems will be much more severe than that in the above-mentioned centralized CF systems.

To fill the research gap, we propose a distributed CF system driven by multicarrier-division duplex (MDD) mode, which enables the FD operation in the same time slot and the same frequency band but at different subcarriers. In the system under study, the subcarriers of one band are divided into two mutually exclusive subsets, namely, a DL and a UL subcarrier subset to support DL and UL transmissions, respectively. Despite the fact that MDD-CF systems suffer from the similar problems of SI and CLI in analog domain as IBFD-CF systems, it can be free from digital-domain SI and CLI with the aid of the FFT operation at the receiver, since interference and desired signal are transmitted over orthogonal subcarriers [10]. In this case, leveraging the existing methods in analog domain, such as power allocation and antenna polarization [4, 12], and the FFT operation in the digital domain, the CLI and SI can be individually mitigated at each AP and MS node, which makes it possible to enable FD-style distributed systems.

However, the power allocation in FD-style CF systems is non-convex and computationally challenging due to the large size of optimization variables. To date, many optimization algorithms for resource allocation have been proposed, such as Dinkelbach's transform [16], quadratic transform (QT) [17, 18], dual decomposition [19] and successive convex approximation (SCA) [20, 21]. These approaches can generally converge to local optimum within several iterations, but their computational complexity expands exponentially as the size of network. Also, once the network is changed, these algorithms need to be re-implemented at the expense of extra computational effort and latency. Therefore, traditional methods can not be implemented in a timely manner for power allocation in CF systems, not to mention the more complicated FD scenarios.

Recently, machine learning (ML) has shown promising success in power allocation of wireless communication systems. In [22], a convolutional neural network (CNN)-based

power allocation model was proposed and shown to superior to the conventional weighted minimum mean square error (WMMSE) method in terms of SE performance and computation time. In [23], authors proposed an ensemble power allocation network (ePCNet) consisting of multiple independent multi-layer fully connected neural networks. The ePCNet is demonstrated to outperform state-of-the-art power allocation solutions such as WMMSE and greedy power allocation. Furthermore, in [24] and [25], deep reinforcement learning-based power allocation was leveraged to deal with the max-min and SE maximization power allocation problem in CF mMIMO systems, respectively. In [26], authors resorted to deep CNN to maximize SE in CF mMIMO systems, which outperforms the well-known use-and-then-forget-based power allocation. In [27], a clustered DNN model based on large-scale fading information was used to implement power allocation in CF mMIMO systems, and its performance is shown to be comparable to that of the WMMSE-alternating direction method of multipliers.

However, although the aforementioned learning-based power allocation was shown to prevail over the traditional methods, they fails to exploit the structure of the wireless communication networks, and hence can not be generalized to unseen scenarios such as varying network sizes or AP/MS density. To this end, graph neural network (GNN) reaping the advantages of scalability, generalization and parallel execution has attracted significant interests from researchers working in wireless communications. In [28], a wireless channel graph convolution network (WCGCN) was proposed for dealing with power allocation and beamforming problem in device-to-device (D2D) systems. Authors showed that the WCGCN trained on small size system can be generalized to a large system with higher density of MS and larger cell sizes. Additionally, [29] and [30] studied the power allocation in ad hoc networks based on GNN. Nevertheless, above papers only exploited the homogeneous GNN in ad hoc or D2D networks with only one type of nodes, which cannot meet the demand of more complicated scenario like FD-CF networks, where AP and MS are two different node types employed with different node features, and each of node is connected with two different types of node via communication path and interference path.

Against this background, we propose a CF-heterogeneous GNN (HGNN) network, namely CF-HGNN, to solve the power allocation problem in distributed MDD-CF systems, which is to the best of our knowledge the first HGNN-based network to handle the power allocation in multicarrier FD-style mMIMO systems.

## B. Contributions

The major contributions are summarized as follows:

- We integrate the MDD mode into the CF systems to enable the FD-style operation in distributed CF multicarrier mMIMO systems, where each AP individually implements DL/UL ZF beamforming. The

SE maximization problem in terms of power allocation is formulated, where the QoS requirements is considered and the effect of residual SI, CLI are practically modeled.

- For the sake of generalization and less complexity, we propose CF-HGNN to deal with the formulated problem. The CF-HGNN can handle varying number of APs, MSs and subcarriers through an adaptive node embedding layer. Furthermore, the message passing algorithm combined with the meta-path attention mechanism is introduced in CF-HGNN, which is able to learn the importance of interfering path and data transmission path during information aggregation at each AP/MS node.
- We conduct comprehensive experiments to evaluate the effectiveness of CF-HGNN for power allocation problem in MDD-CF mMIMO systems. The training of CF-HGNN is implemented in a unsupervised way with unlabeled data. Simulation results show that CF-HGNN is capable of learning nearly the same power allocation strategy with quadratic transform and successive convex approximation (QT-SCA) algorithm and significantly outperforms the traditional unfair greedy method, without any prior information. Additionally, CF-HGNN is adaptive to varying number of nodes and subcarriers, and also generalization ability to different sizes of CF network. Finally, it is demonstrated that CF-HGNN has an incredible advantage over QT-SCA in terms of computational complexity and operation time.

The rest of the paper is organized as follows. In Section II, we propose MDD-CF distributed mMIMO systems, and formulate the SE maximization problem in terms of power allocation. In Section III, the CF-HGNN is proposed to solve the formulated problem in MDD-CF mMIMO systems from a learning perspective. Simulation results are presented in Section IV, and finally, conclusions are drawn in Section V.

## II. SYSTEM MODEL

An MDD-CF mMIMO system is presented, as shown in Fig. 1, where the set  $\mathcal{D} = \{1, \dots, d, \dots, D\}$  of single-antenna MSs and the set  $\mathcal{L} = \{1, \dots, l, \dots, L\}$  of APs of each with  $N$  antennas operate in the MDD mode that rely on the mutually orthogonal subcarrier sets [31], i.e.,  $\mathcal{M} = \{1, \dots, m, \dots, M\}$  with  $|\mathcal{M}| = M$  and  $\bar{\mathcal{M}} = \{1, \dots, \bar{m}, \dots, \bar{M}\}$  with  $|\bar{\mathcal{M}}| = \bar{M}$ , for DL and UL, respectively. The total number of subcarriers is  $M_{\text{sum}} = M + \bar{M}$ . Furthermore, we assume that the CF system operates in a distributed manner, where CPU offloads most of the tasks to APs to relieve its computation burden, and only sends coded data to APs for DL transmissions or integrates the received UL data from APs via fronthaul links without any knowledge of channel information.

### A. Channel Model

For the convenience of notation, we denote the SI channel at the  $l$ -th AP and  $d$ -th MS by  $\mathbf{H}_{ld} \in \mathbb{C}^{N \times N}$  and  $h_{dd}$ ,

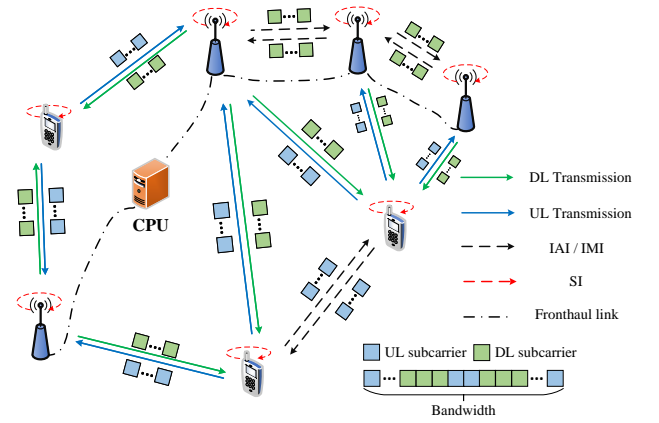


Fig. 1. Illustration of MDD-CF networks.

respectively. These two SI channels are modeled as

$$(\mathbf{H}_{ld})_{i,j} = \sqrt{\xi_l^{\text{SI}}} \alpha_s, \quad h_{dd} = \sqrt{\xi_d^{\text{SI}}} \alpha_s \quad (1)$$

where  $\alpha_s \sim \mathcal{CN}(0, 1)$  is the small-scale fading,  $\xi_l^{\text{SI}}$  and  $\xi_d^{\text{SI}} \in (0, 1]$  denote the residual SI level at AP and MS receivers, respectively.

Furthermore, we denote the time-domain channel impulse responses (CIRs) of the communication channels between the  $d$ -th MS and the  $n$ -th antenna at the  $l$ -th AP, the inter-AP interference (IAI) channels between the  $n$ -th antenna at the  $l$ -th AP and the  $n'$ -th antenna at the  $l'$ -th AP, and the inter-MS interference (IMI) channels between the  $d$ -th MS and  $d'$ -th MS by  $\mathbf{g}_{ld}^n \in \mathbb{C}^{U \times 1}$ ,  $\mathbf{g}_{ll'}^{nn'} \in \mathbb{C}^{U \times 1}$  and  $\mathbf{g}_{dd'} \in \mathbb{C}^{U \times 1}$ , respectively, where  $U$  is the number of taps of multipath channels. Specifically, the  $u$ -th tap of these channels can be generally modeled as  $(\mathbf{g})_u = \sqrt{\beta/U} \alpha_s$  with  $\mathbf{g} \in \{\mathbf{g}_{ld}^n, \mathbf{g}_{ll'}^{nn'}, \mathbf{g}_{dd'}\}$ , where  $\beta \in \{\beta_{ld}, \beta_{ll'}, \beta_{dd'}\}$  accounts for the large-scale fading of path loss and shadowing. Different channel taps are assumed to be independent. Given the time-domain CIRs, the frequency-domain channels can be obtained as  $\mathbf{h} = \mathbf{F}\Psi\mathbf{g}$  with  $\mathbf{h} \in \{\mathbf{h}_{ld}^n, \mathbf{h}_{ll'}^{nn'}, \mathbf{h}_{dd'}\}$ , where  $\mathbf{F} \in \mathbb{C}^{M_{\text{sum}} \times M_{\text{sum}}}$  is the FFT matrix,  $\Psi \in \mathbb{C}^{M_{\text{sum}} \times U}$  is constructed by the first  $U$  columns of  $\mathbf{I}_{M_{\text{sum}}}$ . Moreover, the single DL/UL subcarrier channel can be expressed as  $h[m] = \phi_{\text{DL}}^T \mathbf{h}$  and  $h[\bar{m}] = \phi_{\text{UL}}^T \mathbf{h}$ , respectively, where  $\phi_{\text{DL}} = \mathbf{I}_{M_{\text{sum}}}^{(:,m)}$  and  $\phi_{\text{UL}} = \mathbf{I}_{M_{\text{sum}}}^{(:,bar{m})}$  are the mapping vectors.

### B. Downlink Transmission

The data transmitted on the  $m$ -th DL subcarrier for the  $d$ -th MS is denoted by  $x_d[m]$ , which satisfies  $\mathbb{E}\{|x_d[m]|^2\} = 1$ . The transmitted signal on the  $m$ -th DL subcarrier by the  $l$ -th AP is given by

$$\mathbf{s}_l[m] = \sum_{d \in \mathcal{D}} \sqrt{p_{ldm}} \mathbf{f}_{ld} x_d[m] \quad (2)$$

where  $\mathbf{f}_{ld}[m] \in \mathbb{C}^{N \times 1}$  denotes the precoding vector with  $\|\mathbf{f}_{ld}[m]\|_2^2 = 1$ , and  $p_{ldm}$  is the power allocated to the  $m$ -th subcarrier of the  $d$ -th MS. The total power budget at the

$l$ -th AP is expressed as  $P_l$ , satisfying  $\sum_{m \in \mathcal{M}} \sum_{d \in \mathcal{D}} p_{ldm} \leq P_l$ .

The signal received from the  $m$ -th DL subcarrier at the  $d$ -th MS can be expressed as

$$y_d[m] = \sum_{l \in \mathcal{L}} \mathbf{h}_{ld}^H[m] \mathbf{s}_l[m] + z_d^{\text{SI}} + z_d^{\text{IMI}} + n_d \quad (3)$$

where  $n_d \sim \mathcal{CN}(0, \sigma^2)$  is the additive white Gaussian noise. According to [32, 33], the residual interference in the digital domain arising from SI and IMI (i.e.,  $z_d^{\text{SI}}$  and  $z_d^{\text{IMI}}$  in (3)) are modeled as Gaussian noise [32]. Specifically,  $z_d^{\text{SI}} \sim \mathcal{CN}(0, \mathbb{E}[\bar{z}_d^{\text{SI}} (\bar{z}_d^{\text{SI}})^*])$  with  $\bar{z}_d^{\text{SI}} = h_{dd} \sum_{\bar{m} \in \bar{\mathcal{M}}} \sqrt{p_{d\bar{m}}} x_d[\bar{m}]$ , where  $x_d[\bar{m}]$  denotes the data transmitted on the  $\bar{m}$ -th UL subcarrier by the  $d$ -th MS,  $p_{d\bar{m}}$  denotes the transmitted power.  $z_d^{\text{IMI}} \sim \mathcal{CN}(0, \xi_d^{\text{IMI}} \mathbb{E}[\bar{z}_d^{\text{IMI}} (\bar{z}_d^{\text{IMI}})^*])$  with  $\bar{z}_d^{\text{IMI}} = \sum_{d' \in \mathcal{D} \setminus \{d\}} \sum_{\bar{m} \in \bar{\mathcal{M}}} \sqrt{p_{d'\bar{m}}} h_{dd'}[\bar{m}] x_{d'}[\bar{m}]$ , where  $\xi_d^{\text{IMI}}$  denotes the residual IMI level at MS  $d$ .

Based on (3), it can be shown that the received SINR on the  $m$ -th DL subcarrier at the  $d$ -th MS is given by

$$\text{SINR}_{d,m} = \frac{\sum_{l \in \mathcal{L}} \sqrt{p_{ldm}} \mathbf{h}_{ld}^H[m] \mathbf{f}_{ld}[m]^2}{\text{MUI}_{d,m} + \text{var}\{z_d^{\text{SI}}\} + \text{var}\{z_d^{\text{IMI}}\} + \sigma^2} \quad (4)$$

where  $\text{MUI}_{d,m} = \sum_{l \in \mathcal{L}} \sum_{d' \in \mathcal{D} \setminus \{d\}} p_{ld'm} |\mathbf{h}_{ld'}^H[m] \mathbf{f}_{ld'}[m]|^2$ .

### C. Uplink Transmission

The received UL signal by the  $l$ -th AP from the  $\bar{m}$  subcarrier of MS  $d$  can be expressed as

$$\mathbf{y}_l[\bar{m}] = \sum_{d \in \mathcal{D}} \sqrt{p_{d\bar{m}}} \mathbf{h}_{ld}[\bar{m}] x_d[\bar{m}] + \mathbf{z}_l^{\text{SI}} + \mathbf{z}_l^{\text{IAI}} + \mathbf{n}_l \quad (5)$$

where  $p_{d\bar{m}}$  denotes the power allocated by MS  $d$  to the  $\bar{m}$ -th UL subcarrier, which satisfies  $\sum_{\bar{m} \in \bar{\mathcal{M}}} p_{d\bar{m}} \leq P_d$ . Similar to the received signals at MSs, the residual interference due to the SI and IAI are modeled as Gaussian noise, where  $\mathbf{z}_l^{\text{SI}} \sim \mathcal{CN}(0, \text{diag}(\mathbb{E}[\bar{\mathbf{z}}_l^{\text{SI}} (\bar{\mathbf{z}}_l^{\text{SI}})^H]))$  with  $\bar{\mathbf{z}}_l^{\text{SI}} = \mathbf{H}_l \sum_{m \in \mathcal{M}} \mathbf{s}_l[m]$ , and  $\mathbf{z}_l^{\text{IAI}} \sim \mathcal{CN}(0, \xi_l^{\text{IAI}} \text{diag}(\mathbb{E}[\bar{\mathbf{z}}_l^{\text{IAI}} (\bar{\mathbf{z}}_l^{\text{IAI}})^H]))$  with  $\bar{\mathbf{z}}_l^{\text{IAI}} = \sum_{l' \in \mathcal{L} \setminus \{l\}} \sum_{m \in \mathcal{M}} \mathbf{H}_{ll'}[m] \mathbf{s}_{l'}[m]$ , where  $\xi_l^{\text{IAI}}$  denotes the residual IAI level at the AP side.

Due to the distributed operation in our proposed system, each AP firstly processes the received signal from MSs using local combining vectors, namely  $\tilde{\mathbf{y}}_l[\bar{m}] = \mathbf{w}_{ld}^H[\bar{m}] \mathbf{y}_l[\bar{m}]$ , where  $\mathbf{w}_{ld}[\bar{m}]$  denotes the local combining vector of AP  $l$  for detecting MS  $d$ . Then, the local estimated data of all APs are further collected by the CPU for final processing, which can be expressed as  $y_{\text{cpu}}[\bar{m}] = \sum_{l \in \mathcal{L}} \tilde{\mathbf{y}}_l[\bar{m}]$ . It can be shown that the SINR at CPU when detecting the data transmitted on the UL subcarrier  $\bar{m}$  of MS  $d$  can be expressed as

$$\text{SINR}_{d,\bar{m}} = \frac{p_{d\bar{m}} |\tilde{\mathbf{w}}_d[\bar{m}] \tilde{\mathbf{h}}_d[\bar{m}]|^2}{\text{MUI}_{d,\bar{m}} + \text{SI}_{d,\bar{m}} + \text{IAI}_{d,\bar{m}} + \sigma^2 \|\tilde{\mathbf{w}}_d[\bar{m}]\|^2} \quad (6)$$

where  $\tilde{\mathbf{w}}_d[\bar{m}] = [\mathbf{w}_{1d}^H[\bar{m}], \dots, \mathbf{w}_{Ld}^H[\bar{m}]]$ ,  $\text{SI}_{d,\bar{m}} = \sum_{l \in \mathcal{L}} \mathbb{E}[\|\mathbf{w}_{ld}^H[\bar{m}] \mathbf{z}_l^{\text{SI}}\|^2]$ ,  $\tilde{\mathbf{h}}_d[\bar{m}] = [\mathbf{h}_{1d}^H[\bar{m}], \dots, \mathbf{h}_{Ld}^H[\bar{m}]]^H$ ,  $\text{IAI}_{d,\bar{m}} = \sum_{l \in \mathcal{L}} \mathbb{E}[\|\mathbf{w}_{ld}^H[\bar{m}] \mathbf{z}_l^{\text{IAI}}\|^2]$ ,  $\text{MUI}_{d,\bar{m}} = \sum_{d' \in \mathcal{D} \setminus \{d\}} p_{d'\bar{m}} |\tilde{\mathbf{w}}_d[\bar{m}] \tilde{\mathbf{h}}_{d'}[\bar{m}]|^2$ .

### D. Beamforming Strategy

In this paper, the ZF beamforming strategy is chosen for transmitting and receiving at APs. Generally speaking, MMSE beamforming outperforms ZF beamforming when perfect CSI is available, but when considering the multi-MS interference suppression, computation complexity as well as concise formulation, ZF is used in the following analysis, and it can be easily substituted by MMSE in our proposed network.

According to the ZF principle [34], the precoder/combiner at the  $l$ -th AP, i.e.,  $\mathbf{F}_l^{\text{ZF}}[m] = [\mathbf{f}_{l1}^{\text{ZF}}[m], \dots, \mathbf{f}_{lD}^{\text{ZF}}[m]]$  and  $\mathbf{W}_l^{\text{ZF}}[\bar{m}] = [\mathbf{w}_{l1}^{\text{ZF}}[\bar{m}], \dots, \mathbf{w}_{lD}^{\text{ZF}}[\bar{m}]]$ , can be derived as  $\mathbf{F}_l^{\text{ZF}}[m] = \mathbf{H}_l^H[m] (\mathbf{H}_l[m] \mathbf{H}_l^H[m])^{-1}$  and  $\mathbf{W}_l^{\text{ZF}}[\bar{m}] = \mathbf{H}_l[\bar{m}] (\mathbf{H}_l^H[\bar{m}] \mathbf{H}_l[\bar{m}])^{-1}$ , respectively, where  $\mathbf{H}_l[m] = [\mathbf{h}_{l1}[m], \dots, \mathbf{h}_{lD}[m]]^H$ ,  $\mathbf{H}_l[\bar{m}] = [\mathbf{h}_{l1}[\bar{m}], \dots, \mathbf{h}_{lD}[\bar{m}]]$ . Note that, in order to ensure that the MUI is fully suppressed, the implementation of ZF beamforming should adhere to the constraint of  $N \geq D$ . In this case, the MUI terms in (4) and (6) are equal to zero. Therefore, the  $\text{SINR}_{d,m}$  and  $\text{SINR}_{d,\bar{m}}$  can be rewritten as follows

$$\begin{aligned} \text{SINR}_{d,m} &= \frac{|\sum_{l \in \mathcal{L}} \sqrt{p_{ldm}} \omega_{ldm}|^2}{\xi_d^{\text{SI}} \Theta_{\text{DL}} + \sigma^2} \\ \text{SINR}_{d,\bar{m}} &= \frac{p_{d\bar{m}} L^2}{\sum_{l \in \mathcal{L}} v_{ld\bar{m}} (\xi_l^{\text{SI}} \Theta_{\text{UL}} + \sigma^2)} \end{aligned} \quad (7)$$

where  $\omega_{ldm} = 1/\|\mathbf{f}_{ld}^{\text{ZF}}[m]\|_2$ ,  $v_{ld\bar{m}} = \|\mathbf{w}_{ld}^{\text{ZF}}[\bar{m}]\|_2^2$ ,  $\Theta_{\text{DL}} = \sum_{\bar{m} \in \bar{\mathcal{M}}} p_{d\bar{m}} + \sum_{d' \in \mathcal{D} \setminus \{d\}} \sum_{\bar{m} \in \bar{\mathcal{M}}} (\xi_d^{\text{IMI}} \beta_{dd'} p_{d'\bar{m}} / \xi_d^{\text{SI}} M_{\text{sum}})$ ,  $\Theta_{\text{UL}} = \sum_{m \in \mathcal{M}} \sum_{d \in \mathcal{D}} p_{ldm} + \sum_{l' \in \mathcal{L} \setminus \{l\}} \sum_{m \in \mathcal{M}} \sum_{d \in \mathcal{D}} (\xi_l^{\text{IAI}} \beta_{ll'} p_{l'dm} / \xi_l^{\text{SI}} M_{\text{sum}})$ . For the details of simplification, please refer to Appendix A.

### E. Problem Formulation

Given the  $\text{SINR}_{d,m}$  and  $\text{SINR}_{d,\bar{m}}$  derived in (7), the optimization problem can be formulated as follows:

$$\max_{p_{ldm}, p_{d\bar{m}}} \Lambda_{\text{SE}} \quad (8a)$$

$$\text{s.t.} \quad \sum_{m \in \mathcal{M}} \sum_{d \in \mathcal{D}} p_{ldm} \leq P_l, \quad \forall l \in \mathcal{L} \quad (8b)$$

$$\sum_{\bar{m} \in \bar{\mathcal{M}}} p_{d\bar{m}} \leq P_d, \quad \forall d \in \mathcal{D} \quad (8c)$$

$$\sum_{m \in \mathcal{M}} \ln(1 + \text{SINR}_{d,m}) \geq \chi_{\text{DL}}, \quad \forall d \in \mathcal{D} \quad (8d)$$

$$\sum_{\bar{m} \in \bar{\mathcal{M}}} \ln(1 + \text{SINR}_{d,\bar{m}}) \geq \chi_{\text{UL}}, \quad \forall d \in \mathcal{D} \quad (8e)$$

where  $\Lambda_{\text{SE}} = \frac{1}{M_{\text{sum}}} \sum_{d \in \mathcal{D}} (\sum_{m \in \mathcal{M}} \ln(1 + \text{SINR}_{d,m}) + \sum_{\bar{m} \in \bar{\mathcal{M}}} \ln(1 + \text{SINR}_{d,\bar{m}}))$ ,  $\chi_{\text{DL}}$  and  $\chi_{\text{UL}}$  denote DL and UL QoS requirements respectively. It can be observed that (8) is a NP-hard nonconvex problem with nonconvex constraints as shown in (8d) and (8e).

## III. GRAPH LEARNING IN MDD-CF NETWORK

In order to leverage the structural information of CF network to deal with the complicated problem, as formulated in (8), the heterogeneous graph learning based

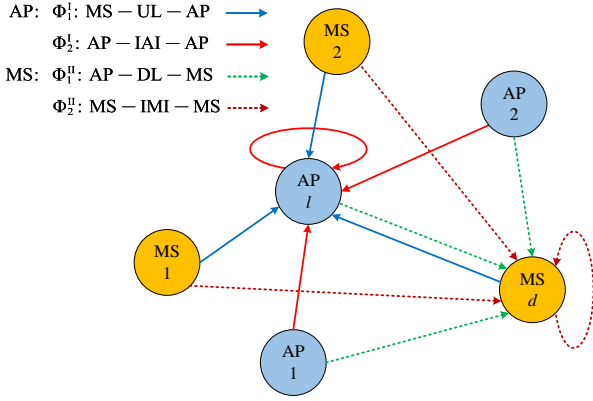


Fig. 2. An example graph of CF network.

power allocation scheme is introduced. We aim to learn a scalable and transferable HGNN to efficiently distribute both APs and MSs transmit power to maximize the sum rate of MDD-CF networks.

### A. Definition of Heterogeneous Graph

A heterogeneous graph can be represented as  $G = (\mathcal{V}, \mathcal{E})$ , where  $\mathcal{V}$  is the set of nodes, and  $\mathcal{E}$  is the set of edges. The heterogeneous graph has a node type mapping function  $\phi: \mathcal{V} \rightarrow \mathcal{Q}$  and an edge type mapping function  $\psi: \mathcal{E} \rightarrow \mathcal{P}$ , where  $\mathcal{Q}$  and  $\mathcal{P}$  denote the sets of predefined node types and link types with  $|\mathcal{Q}| + |\mathcal{P}| > 2$  [35]. The  $\mathbf{v} \in \mathbb{R}^{F_v \times 1}$  denotes a node with  $F_v$ -dimensional features and the  $\mathbf{e}_{i,j} \in \mathbb{R}^{F_e \times 1}$  denotes an edge pointing from  $\mathbf{v}_j$  to  $\mathbf{v}_i$  with  $F_e$ -dimensional features. Given mapping function  $\phi$  and  $\psi$ , each node belongs to a particular node type  $\phi(\mathbf{v}) \in \mathcal{Q}$  and each edge belongs to a specific relation  $\psi(\mathbf{e}) \in \mathcal{P}$ . The neighborhood of a node  $\mathbf{v}_i$  is defined as  $\mathcal{N}_i = \{\mathbf{v}_j \in \mathcal{V} | \mathbf{e}_{i,j} \in \mathcal{E}\}$ . Furthermore, in a heterogeneous graph, two nodes can be connected via different semantic paths. For example, APs and MSs are connected via two paths, i.e., AP-DL-MS and MS-UL-AP links. Therefore, here we introduce the definition of meta-path in [36]. A meta-path  $\Phi$  is defined as a path in the form of  $Q_1 \xrightarrow{P_1} Q_2 \xrightarrow{P_2} \dots \xrightarrow{P_n} Q_{n+1}$ , which defines a composite relation  $P = P_1 \circ P_2 \circ \dots \circ P_n$  between types  $Q_1$  and  $Q_{n+1}$ , where  $\circ$  denotes the composition operator on relations. Once a meta-path  $\Phi$  is given, the specific neighbors  $\mathcal{N}_i^\Phi$  of node  $\mathbf{v}_i$  is obtained, which is defined as the set of nodes connected with  $\mathbf{v}_i$  via meta-path  $\Phi$ .

### B. MDD-CF Heterogeneous Graph

Intuitively, as shown in Fig. 2, it is straightforward to model an MDD-CF network as a heterogeneous graph. It can be observed from the figure that there are two types of nodes, i.e., AP and MS, and each of them is associated with two meta-paths. Specifically, as for AP  $l$ , all MSs are connected with it via meta-path  $\Phi_1^I$  (MS-UL-AP), and the remaining APs are connected with it via meta-path  $\Phi_2^I$  (AP-IAI-AP). Note that, the SI caused by AP  $l$  itself

is classified into  $\Phi_2^I$  by adding a self-loop. Similarly, meta-paths  $\Phi_1^{II}$  and  $\Phi_2^{II}$  associated with MS  $d$  refer to links AP-DL-MS and MS-IMI-MS, respectively.

The node feature vectors of AP  $l$  and MS  $d$  are given by

$$\begin{aligned} \mathbf{v}_l &\in \mathbb{R}^{(DM+3) \times 1} = [\boldsymbol{\omega}_{l1}^T \dots \boldsymbol{\omega}_{lM}^T, P_l, \xi_l^{\text{SI}}, \xi_l^{\text{IAI}}]^T, \\ \mathbf{v}_d &\in \mathbb{R}^{(LM+3) \times 1} = [\mathbf{v}_{1d}^T \dots \mathbf{v}_{Md}^T, P_d, \xi_d^{\text{SI}}, \xi_d^{\text{IMI}}]^T \end{aligned} \quad (9)$$

respectively, where  $\boldsymbol{\omega}_{lm} = [\omega_{l1m}, \dots, \omega_{lDm}]^T$  is the  $m$ -th DL equivalent subchannel gains between AP  $l$  and all the MSs, and  $\mathbf{v}_{\bar{m}d} = [v_{1d\bar{m}}, \dots, v_{LD\bar{m}}]^T$  is the  $\bar{m}$ -th UL equivalent subchannel gains between MS  $d$  and all the APs, when ZF beamforming is applied as in equation (7). Moreover, to simplify the model for the sake of low complexity, the attribute of edges is assumed to be the Euclidean distance between any of two nodes, i.e.,  $e_{i,j} = d_{i,j}, \forall i, j \in \mathcal{V}$ . If  $i = j, e_{i,j} = 0$  denoting the edge feature of self-loop.

*Remark 1.* In the distributed CF systems, each AP equipped with a baseband processor is able to independently implement DL/UL beamforming, while the CPU only need to make final data detection. Hence, in order to avoid using lengthy channel vectors for the sake of low feature dimensions of both AP and MS nodes, we assume that each AP first computes equivalent DL/UL subchannel gains based on CSI, which are subsequently transmitted to the CPU as the AP/MS node features during offline graph training. Note that in several papers like [37], authors used the geographic location information (GLI) as the input of learning-based networks to reduce the training overhead. It is thus to use GLI as the AP/MS node features, thereby avoiding the computation of beamforming. However, in our paper, since power needs to be allocated among different subcarriers, GLI obviously fails to contain the small-scale information of wireless links and hence can not be used in multicarrier systems.

### C. Heterogeneous Graph learning Based Power Allocation for MDD-CF Network

In this subsection, we formally present the CF-HGNN to solve the power allocation problem in MDD-CF networks. The architecture of CF-HGNN consists of four components: 1) adaptive node embedding; 2) meta-path based message passing; 3) meta-path based attention; 4) downstream power allocation learning. The overall network is type-specific and the parameters for processing AP and MS nodes are not shared.

1) *Adaptive Node Embedding:* Generally, in order to guarantee the scalability of GNN, the size of node feature should be irrelevant to the number of nodes. As we can see in (9), the feature dimension of input nodes related to  $L$  and  $D$  vary in different scale of CF networks, which makes it infeasible to exhibit the scalability and transferability<sup>1</sup>. To tackle this problem, we propose an adaptive node

<sup>1</sup>We assume that the number of available DL/UL subcarriers remains consistent, as the number of APs and MSs changes, and vice versa.



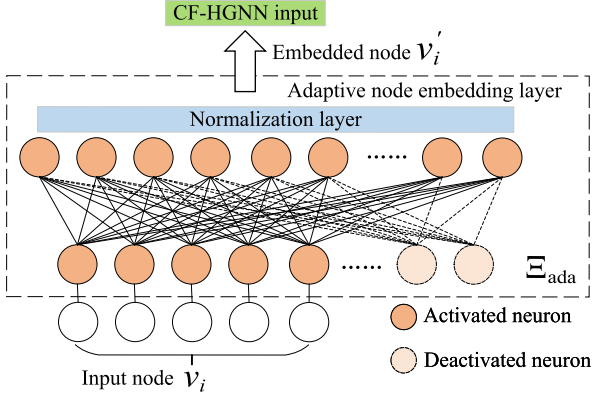


Fig. 3. Adaptive node embedding layer.

embedding layer, which can map one type of nodes to the same feature domain through adaptively activating or deactivating the neurons in multi-layer perceptron (MLP), i.e.,  $\Xi_{\text{ada}}$ , as depicted in Fig. 3. Note that AP and MS nodes are transformed by two embedding layer matrices, i.e.,  $\mathbf{v}'_l = \mathbf{W}'_{\text{AP}}(:, 1:DM+3)\mathbf{v}_l$  and  $\mathbf{v}'_d = \mathbf{W}'_{\text{MS}}(:, 1:LM+3)\mathbf{v}_d$ , where  $\mathbf{W}'_{\text{AP}} \in \mathbb{R}^{F_{\text{AP}} \times F_{\text{AP}}}$  and  $\mathbf{W}'_{\text{MS}} \in \mathbb{R}^{F'_{\text{MS}} \times F_{\text{MS}}}$ . Note that as the ZF beamforming is applied, the maximum input size of embedding layer for AP nodes is subject to the number of antennas employed at APs, i.e.,  $F_{\text{AP}} = NM + 3$ . Also, AP density leads to  $F'_{\text{MS}} = L'\bar{M} + 3$ , where  $L'$  denotes the maximum number of APs that can be deployed in CF networks.

*Remark 2.* Our CF-HGNN model imposes strict limitation on the number of MSs. In other word, the number of MSs can only vary within the number of antennas configured at each AP. If MSs are densely distributed, or each AP is only configured with few antennas, the node features can no longer be set as (9), since the equivalent subchannel gain is unavailable with ZF beamforming under the assumption of  $N \ll D$ . To this end, extra pre-processing implementation should be considered. One possible method is to build user-centric clustering [1], where each MS can be assigned to different number of APs and each AP only serves a fixed number of MSs. For example, if ZF beamforming is used, each AP can serve up to  $N$  MSs depending on channel conditions. Accordingly, the dimension of node features is still only related to the number of antennas. To stay focused, we only consider the case of  $N \geq D$ , and the user-centric clustering will be considered in future research.

2) *Meta-path Based Message Passing:* According to the example shown in Fig. 2, each AP/MS node connects neighboring nodes via two meta-paths, and all the meta-paths are mutually independent. Hence, within each meta-path  $\Phi$ , the process of message passing from neighboring nodes to central nodes is formulated as follows:

$$\mathbf{z}_i^\Phi = \text{Mean} \left( \Xi_2 \left( \mathbf{v}'_i \oplus \frac{1}{|\mathcal{N}_i^\Phi|} \Xi_1 \left( \sum_{j \in \mathcal{N}_i^\Phi} \mathbf{v}'_j \cdot e_{i,j} \right) \right) + \underset{\text{Res}}{\mathbf{v}'_i} \right) \quad (10)$$

where  $\Xi_1$  and  $\Xi_2$  are two different MLPs including fully-connected, activation and normalization layers,  $\text{Res } \mathbf{v}'_i$

denotes the residual connection, which can maintain the original node information after multi-layer message passing,  $\oplus$  is the concatenation operation.

3) *Meta-path Based Attention:* Generally, the information update at each AP/MS node relies on the interfering path and data transmission path. However, the impact of two paths on each node is quite different. For instance, if an AP node is closely surrounded by MS nodes and other AP nodes are far away from it, the meta-path  $\Phi_1^I$  is more important than  $\Phi_2^I$ , and vice versa. Based on this observation, we propose meta-based attention to enable networks to automatically learning the importance of two meta-paths. An example of calculating the attention vector at AP node is shown as follows:

$$\alpha_{\Phi_1^I} = \frac{1}{L} \sum_{l \in \mathcal{L}} \mathbf{q}^T \Xi_{\text{att}}(\mathbf{z}_l^{\Phi_1^I})$$

$$\beta_{\Phi_1^I} = \frac{\exp(\alpha_{\Phi_1^I})}{\exp(\alpha_{\Phi_1^I}) + \exp(\alpha_{\Phi_2^I})} \quad (11)$$

where  $\Xi_{\text{att}}$  is the MLP layer for attention,  $\mathbf{q}$  is the learnable attention vector,  $\mathbf{z}_l^{\Phi_1^I}$  denotes the aggregated information via meta-path  $\Phi_1^I$ . Then, the final node representation of AP  $l$  is  $\mathbf{z}_l = \beta_{\Phi_1^I} \mathbf{z}_l^{\Phi_1^I} + \beta_{\Phi_2^I} \mathbf{z}_l^{\Phi_2^I}$ . Similarly, we can obtain the  $\mathbf{z}_d$  at MS  $d$ . It is noteworthy that the process of message passing plus attention can be iteratively implemented for  $K$  times so as to collect the high-hop neighbors, and our proposed model can be termed as  $K$ -th layer CF-HGNN.

4) *Downstream Power Allocation Learning:* After the  $K$ -th iteration, the final representation of AP and MS nodes, i.e.,  $\mathbf{z}_l^{(K)}$  and  $\mathbf{z}_d^{(K)}$  are used for downstream power allocation learning, which can be expressed as:

$$\mathbf{p}_l \in \mathbb{R}^{DM \times 1} = \text{Relu} \left( \Xi_{\text{PA}}(\mathbf{z}_l^{(K)})^{(1:DM)} \right)$$

$$\mathbf{p}_d \in \mathbb{R}^{\bar{M} \times 1} = \text{Relu} \left( \Xi_{\text{PA}}(\mathbf{z}_d^{(K)}) \right) \quad (12)$$

where  $\Xi_{\text{PA}}$  denotes the MLP for power allocation learning, Relu is used to constrain the power to be positive. Corresponding to the adaptive node embedding in part 1), in order to make the network feasible with different number of MSs, the adaptive output layer supports up to  $NM$  DL power allocation values by activating or deactivating the neurons. By contrary, provided that the number of available UL subcarriers is constant, as each MS only needs to allocate UL power, the size of output layer for MS node is fixed to  $\bar{M}$ . The overall architecture of CF-HGNN for AP nodes is shown in Fig. 4, which keeps the same for MS nodes except the size of output layer as mentioned. Also, it is noteworthy that all the MLPs shown in Fig. 4 are AP-specific, which means the MLPs for MSs are different from that for APs.

*Remark 3.* As we assume  $N \geq D$ , to scale down the dimension of node feature thereby reducing training complexity of the CF-HGNN model, we feed the node feature with well-computed equivalent subchannel gains based on ZF beamforming as shown in (9). Other beamforming methods like MMSE or matched filtering can also be used. When few antennas are employed at APs, it is possible

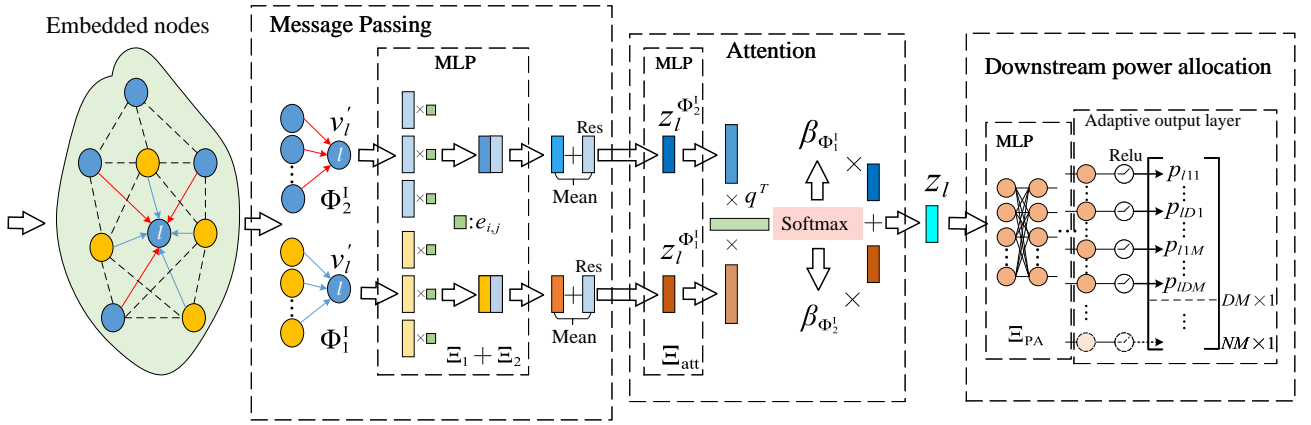


Fig. 4. The overall architecture of CF-HGNN network for AP nodes.

$$\begin{aligned}
 \mathcal{L}(\theta) = \mathbb{E} & \left[ -\Lambda_{SE} + \sum_{d=1}^D \left( \kappa_1 \text{Relu}(\chi_{DL} - \sum_{m \in \mathcal{M}} \ln(1 + \text{SINR}_{d,m})) + \kappa_2 \text{Relu}(\chi_{UL} - \sum_{\bar{m} \in \bar{\mathcal{M}}} \ln(1 + \text{SINR}_{d,\bar{m}})) \right) \right. \\
 & \left. + \kappa_3 \text{Relu} \left( \sum_{\bar{m} \in \bar{\mathcal{M}}} p_{d\bar{m}} - P_d \right) + \sum_{l=1}^L \kappa_4 \text{Relu} \left( \sum_{m \in \mathcal{M}} \sum_{d \in \mathcal{D}} p_{ldm} - P_l \right) \right] \quad (13)
 \end{aligned}$$

to setup AP and MS node features with channel vectors, which have lengths of  $(2DNM + 3)$  and  $(2LN\bar{M} + 3)$ , respectively, considering both real and imaginary parts of complex vectors. In this case, we can directly learn the beamforming vectors at the final output layer, rather than choosing one of known beamforming schemes as the network input. This solution needs to be cooperated with user-centric clustering as mentioned before and the CF-HGNN model has to be modified. The reason is that if the number of MSs and subcarriers are large, the huge dimension of node feature will make model hard to train. We leave this solution to be considered in our next work.

To perform CF-HGNN training in an unsupervised way, we define the loss function as (13), where  $\theta$  denotes the parameters of the neural network and the expectation is taken over all the channel realizations, each ReLU penalty term will have a positive value only if the DL/UL QoS requirements and transmit power budgets are not satisfied, enforcing the training process towards satisfying the given requirement, and the positive parameters  $\kappa_i$  give the different priority to each penalty term.

#### IV. SIMULATION RESULTS

##### A. Simulation Setup

In this section, we evaluate the power allocation performance of our proposed CF-HGNN architecture in terms of system SE. The simulation parameters of MDD-CF network are listed in Table I. As shown in the table, given the AP density and cell length, the maximum number of AP that can be deployed in our proposed CF network is  $L' = 24$ . In addition, the large-scale fading is given by [1]:

$$\beta[\text{dB}] = -30.5 - 36.7 \log_{10}(d) + \sigma_{sh}z \quad (14)$$

where  $d$  denotes the distance between any two nodes,  $\sigma_{sh}z$  is shadow fading with standard deviation of  $\sigma_{sh} = 4$  dB and  $z \sim \mathcal{N}(0, 1)$ . Furthermore, we assume that APs are capable of providing 30 dB IAI suppression in the propagation/analog domain with the existing approaches [4]. Then, provided that the 12-bit ADC is applied, the MDD system can suppress IAI up to 72 dB (i.e.,  $\xi_l^{\text{MDD-IAI}} = -72$  dB,  $\forall l$ ), of which 42 dB is attributed to the digital cancellation by FFT<sup>2</sup>. By contrast, as MSs are of lightweight equipment with single antenna and hardly share the channel knowledge with other MSs, they can not actively suppress IMI. However, similar to APs, MSs are able to cancel 42 dB IMI in the digital domain (i.e.,  $\xi_d^{\text{MDD-IMI}} = -42$  dB,  $\forall d$ ) with the FFT operation [32].

As for neural network setting, we adopt a 2-layer CF-HGNN based on Pytorch Geometric [38]. The general MLPs  $\Xi_1$  and  $\Xi_2$  during message passing process contains several fully-connected linear layers followed by LeakyRelu activation layer and batch normalization layer, while the  $\Xi_{PA}$  belongs to the downstream task layer and has no batch normalization layer. Moreover, the  $\Xi_{ada}$  and  $\Xi_{att}$  are single-layer MLP with only one fully-connected linear layer. As formulated in (13), the overall learning is unsupervised without any ground truth. To optimize the CF-HGNN, we adopt the Adam optimizer with a learning rate of 0.001 [39]. Also, we empirically set  $\kappa_i$  in (13) as  $\{0.1, 1, 0.1, 0.1\}$  during training. As to learning samples,

<sup>2</sup>The 12-bit ADC has a maximum dynamic range of 42dB, which means it can accommodate up to 42dB power of IAI and transform them into digital signal without too much quantization noise. Then, in the digital domain, since the interference signal is transmitted over DL subcarriers, which is mutually orthogonal to the desired UL signal, MDD systems are capable of implementing digital-domain SIC by the FFT operation

TABLE I  
SIMULATION PARAMETERS

Default parameters	Value
AP density	150 AP/km <sup>2</sup>
Cell area ( $S_D \times S_D$ )	400 × 400m
Number of antennas per AP ( $N$ )	8
Number of DL/UL subcarriers ( $M, M$ )	(4, 2)
AP and MS power ( $P_l, P_d, \forall l, d$ )	(40, 30) dBm
QoS requirements ( $\chi_{DL}, \chi_{UL}$ )	(0.5, 0.1) nats/s/Hz
Noise power ( $\sigma^2$ )	-94 dBm
Delay taps ( $U$ )	4
Residual SI level at AP ( $\xi_l^{SI}, \forall l$ )	-120 dB
Residual SI level at MS ( $\xi_d^{SI}, \forall d$ )	-110 dB

we randomly generate 10000 and 1000 CF network layouts for training and testing, respectively, where APs and MSs are uniformly distributed. The batch size for training is 64, and the network parameters are only updated during training, while stay constant during testing. We run CF-HGNN on a GeForce GTX laptop 3080Ti, while other methods is implemented on the 12th Gen Intel(R) Core(TM) i7-12700H 2.70 GHz.

For comparison, we introduce QT-SCA as the main benchmark, which is implemented using the CVX tool during simulations [40]. In addition, greedy unfair allocation method is introduced as another benchmark [41], where water-filling algorithm is used at each AP/MS to distribute all of the power among MSs over DL/UL subcarriers, regardless of the QoS constraints.

### B. Performance Comparison

In this section, we will make a comprehensive performance comparison between different power allocation methods in MDD-CF networks, where the number of MSs and APs in CF networks is fixed during training and testing, and set as  $L = 24, D = 6$ . In this case,  $\Xi_{\text{ada}}$  and  $\Xi_{\text{PA}}$  of CF-HGNN can be seen as identical matrices.

Firstly, we compare QT-SCA, CF-HGNN and greedy unfair methods in terms of SE distribution of 1000 testing CF network layouts. As shown in Fig. 5, CF-HGNN achieves nearly the same performance as QT-SCA in terms of 95%-likely SE. Furthermore, the SE performance gap between QT-SCA and CF-HGNN with regard to each CF network layout is depicted in Fig. 6. It can be observed that the absolute value of SE gap between these two methods is lower than 1.5 nats/s/Hz, and in several layouts, CF-HGNN can outperform QT-SCA, demonstrating that CF-HGNN is capable of learning the near-optimal power allocation strategy in MDD-CF networks. Noticeably, both QT-SCA and CF-HGNN significantly outperform the greedy unfair method. The rationale is that although the latter one can maximize the SE in classic HD-based multiuser OFDM systems [41], it lacks the management of complicated interferences in CF FD-like systems, leading to poor performance at both AP and MS sides.

Next, we randomly select one of CF network layouts in testing samples, as shown in Fig. 7, to dig deeper into the results of power allocation achieved by QT-SCA and CF-HGNN. To make clear drawing in Fig. 7,

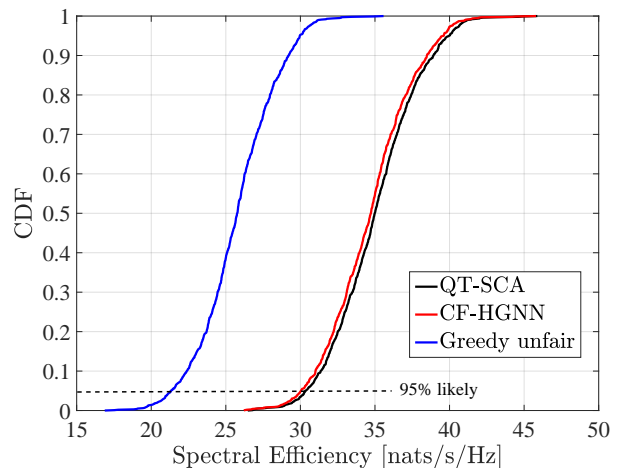


Fig. 5. Cumulative distribution versus SE, where  $L = 24, D = 6$ .

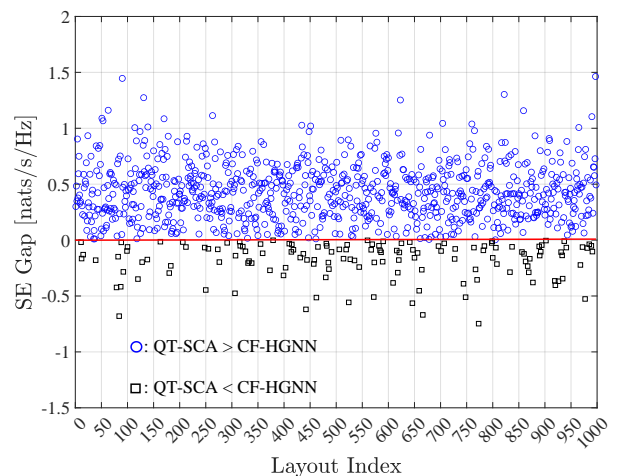


Fig. 6. SE performance gap between QT-SCA and CF-HGNN, where  $L = 24, D = 6$ .

the DL connections between AP and MS with less than 2W transmit power are omitted, and different color lines denote the DL connections obtained by either method or both. Fig. 7 shows that, except MS 6, CF-HGNN and QT-SCA create the same subset of major serving APs for each MS, and obtain the similar results of UL power allocation. As for MS 6, since it situates relatively far away from other APs, in order to meet the demand of DL QoS, more APs are required to transmit power to it. Although varying DL connections are obtained using two methods, there is essentially no difference between them. For example, apart from common connections, CF-HGNN picks AP 3 and 9 to serve MS 6, while QT-SCA chooses AP 8 located between AP 3 and 9. Also, AP 20 and 17 with the similar distance from MS 6 are selected by CF-HGNN and QT-SCA, respectively.

It is worth mentioning that the DL power and UL power used in Fig. 7 are sum of power allocated to DL subcarriers and UL subcarriers, respectively. In Table II, an example of the detailed subcarriers power allocation at AP 1, MS 2 and MS 6 are presented. It can be observed



TABLE II  
SUBCARRIERS POWER ALLOCATION AT AP 1, MS 2 AND MS 6.

Connections	Method	DL subcarriers power (W)				DL power (W)	UL subcarriers power (W)		UL power (W)
AP 1→MS 6, MS 6→APs	QT-SCA	1.89	0.81	1.90	1.89	<b>6.49</b>	0.006	0.008	<b>0.014</b>
	CF-HGNN	1.77	1.74	1.78	1.79	<b>7.08</b>	0.003	0.010	<b>0.013</b>
	Greedy unfair	1.26	1.19	1.25	1.25	<b>4.95</b>	0.499	0.501	<b>1.000</b>
AP 1→MS 2, MS 2→APs	QT-SCA	0.75	0.33	0.49	0.31	<b>1.88</b>	0.026	0.038	<b>0.064</b>
	CF-HGNN	0.25	0.23	0.22	0.27	<b>0.97</b>	0.000	0.117	<b>0.117</b>
	Greedy unfair	0.00	0.00	0.00	0.00	<b>0.00</b>	0.000	1.000	<b>1.000</b>

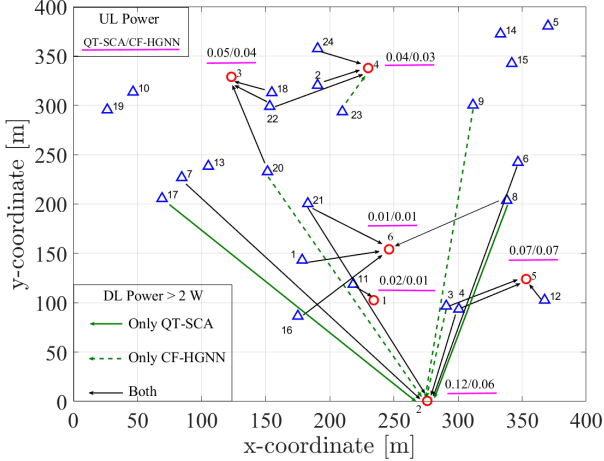


Fig. 7. A MDD-CF network topology, where  $L = 24$ ,  $D = 6$ .

that CF-HGNN and greedy unfair methods achieve more consistent allocation among subcarriers, which means the power is distributed largely on large-scale fading, while QT-SCA has better capability of exploiting the small-scale fading. Moreover, we can see that MS 6 has lower UL transmit power than MS 2 based on the results of CF-HGNN and QT-SCA. The reason behind is that MS 6 is in close proximity to MS 1, the increase of UL transmit power may not only cause more SI on DL reception but also large IMI on MS 1, leading to degradation of SE. By contrast, the greedy unfair scheme implements power allocation only considering the quality of communication channels without regard to the effect of interference.

The performance of different methods in terms of SE, convergence behavior and operation time are plotted in Fig. 8. As expected, QT-SCA and CF-HGNN achieve comparable SE, and their performance gap is only 0.35 nats/s/Hz. Nevertheless, since QT-SCA is an iterative algorithm with very high computational complexity, it converges within 6 iterations and takes 7.03s operation time in total. On the contrary, with the aid of parallel computation of GPU, CF-HGNN is capable of using  $10^4$  times less operation time to reach 99% performance of QT-SCA. In addition, although the greedy fair method costs the similar operation time with CF-HGNN as only water-filling algorithm is applied at both APs and MSs side, its SE performance significantly lags behind the other two methods.

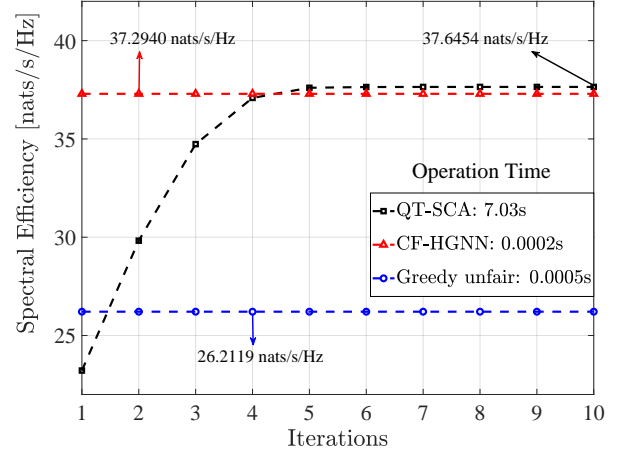


Fig. 8. SE convergence behavior and operation time of different methods, where  $L = 24$ ,  $D = 6$ .

### C. Various Scales of Networks

1) *Adaption to Different Number of Nodes and Subcarriers*: Although the simulation results in Section IV-B demonstrate that CF-HGNN is able to fulfill satisfactory performance as QT-SCA, the overall model is dedicated to the fixed number of nodes and subcarriers in CF networks. Next, we adopt the adaptive node embedding as well as output layers to evaluate the capability of CF-HGNN in dealing with varying networks. We use 10000 samples to train the Dedicated CF-HGNN, which can only be used for the network with specific number of nodes and subcarriers. For fair comparison, we will also use 10000 samples in total consisting of various nodes and subcarriers in networks to train Adaptive CF-HGNN model. Table III shows that by employing adaptive layers, Adaptive CF-HGNN can achieve the relatively stable performance over networks with different nodes and subcarriers, which makes it feasible for dynamic power allocation in MDD-CF networks. On the contrary, QT-SCA and Fixed CF-HGNN have to re-compute the complicated optimization problem or re-train the model so as to response to varying networks. Note that, the SE decreases with the number of subcarriers increases since the power allocated to each subcarrier is reduced and the SE is divided by  $M_{\text{sum}}$  as shown in (8). Apparently, the total SE after multiplying  $M_{\text{sum}}$  is significantly increased thanks to subcarrier diversity.

2) *Generalization to Different Sizes of Cell*: In this part, we evaluate the generalization of the proposed CF-HGNN

TABLE III  
GENERALIZATION TO DIFFERENT NUMBER OF APs, MSs AND SUBCARRIERS. THE RESULTS ARE NORMALIZED BY THE SE OF QT-SCA.

$L$	$D$	$M/\bar{M}$	QT-SCA (nats/s/Hz)	Dedicated CF-HGNN	Adaptive CF-HGNN	Greedy unfair
24	4	4/2	26.42	98.07%	94.14%	74.45%
	5		31.34	98.02%	94.51%	74.06%
	6		34.23	97.78%	94.77%	73.06%
	7		36.24	98.18%	95.45%	73.68%
20	6	4/2	33.04	98.09%	97.22%	72.79%
16			29.99	97.70%	95.07%	71.16%
12			25.69	98.52%	94.08%	69.95%
8			21.13	97.40%	94.46%	68.67%
16	6	32/16	9.26	98.81%	91.58%	72.35%
		16/8	15.53	99.03%	91.50%	68.45%

TABLE IV  
GENERALIZATION TO DIFFERENT SIZES OF CELL. THE RESULTS ARE NORMALIZED BY THE SE OF QT-SCA.

$S_D$	QT-SCA (nats/s/Hz)	Dedicated CF-HGNN	Generalized CF-HGNN
350	37.85	96.64%	95.19%
300	40.64	98.08%	93.13%
250	43.76	98.42%	91.84%
200	46.84	99.91%	91.78%
150	50.10	101.42%	92.79%

model to different sizes of cell. We first use 10000 samples to train the network with  $S_D = 400$ . As shown in Table IV, the Generalized CF-HGNN denotes the results obtained by directly using the well-trained model with  $S_D = 400$ , while the Dedicated CF-HGNN is trained under the specific cell size. It can be observed that as cell size shrinks, the performance of the Generalized CF-HGNN degrades slightly but is still acceptable. However, the Dedicated CF-HGNN finally outperforms the QT-SCA when  $S_D = 150$ , which means CF-HGNN with specific training samples can learn a better power allocation strategy in dense networks.

#### D. Computational Complexity

We finally make a comparison between QT-SCA and CF-HGNN in terms of computation complexity and operation time. The number of APs and subcarriers are fixed, while the number of MSs increases from 4 to 7. According to [42], the approximated computational complexity of QT-SCA can be obtained as  $\mathcal{O}((LDM + 2DM + 3D\bar{M})^2(L + D + 3DM_{\text{sum}})^{2.5} + (L + D + 3DM_{\text{sum}})^{3.5})$  per iteration. As to CF-HGNN, the computational complexity mainly comes from the matrix computation, as shown in (10)-(12). Table V shows that when doubling the number of APs, MSs and subcarriers, the computational complexity of QT-SCA increases much more quickly than that of CF-HGNN. Furthermore, the operation time comparison between QT-SCA and CF-HGNN is plotted in Fig. 9. We can see that CF-HGNN takes significantly less time than QT-SCA, and thanks to the parallel computation of GPU, CF-HGNN with GPU has the best performance in terms of operation time.

## V. CONCLUSIONS

In this paper, we proposed an MDD-CF distributed mMIMO system, and formulated an SE maximization

TABLE V  
COMPUTATIONAL COMPLEXITY COMPARISON

$L$	$D$	$M/\bar{M}$	Methods	
			QT-SCA	CF-HGNN
6	2	4/2	$4.48 \times 10^8$	$6.83 \times 10^6$
12	4	8/4	$4.78 \times 10^{11}$	$2.75 \times 10^7$
24	8	16/8	$6.79 \times 10^{14}$	$1.48 \times 10^8$

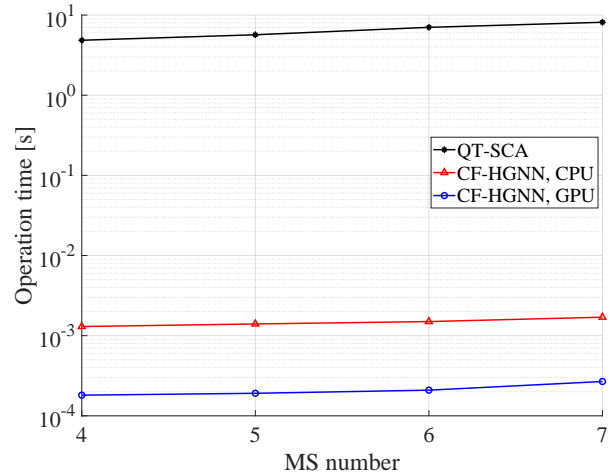


Fig. 9. Operation time comparison between QT-SCA and CF-HGNN.

problem, considering power allocation at both AP and MS sides, as well as QoS requirements. In order to solve the non-convex and NP-hard formulated problem, we introduced the CF-HGNN model to deal with the formulated problem from a learning perspective, which consists of adaptive node embedding layer, meta-based message-passing, meta-based attention mechanism and downstream power allocation learning. The CF-HGNN

is trained in an unsupervised fashion with unlabeled data, which significantly reduces the system overhead. Numerical results showed that CF-HGNN can achieve a comparable SE performance to QT-SCA but with much less operation time and computational complexity. Also, CF-HGNN largely prevails over the unfair greedy method in terms of SE performance. Furthermore, CF-HGNN can handle varying number of APs, MSs and subcarriers, and has generalization ability to different sizes of CF network. In the future research, we aim to integrate the cooperation clustering into CF-HGNN so as to mitigate the restriction on the number of MSs, which is assumed to be less than the number of antennas configured at each AP in this paper.

## APPENDIX A

THE SIMPLIFICATION OF  $\text{SINR}_{d,m}$  AND  $\text{SINR}_{d,\bar{m}}$  IN (7)

For the  $\text{SINR}_{d,m}$ , since the ZF precoder is employed with the constraint of power normalization, the numerator of (4) can be transformed to  $|\sum_{l \in \mathcal{L}} \sqrt{p_{ldm}} \omega_{ldm}|^2$ , where  $\omega_{ldm} = \frac{1}{\|\mathbf{f}_{ld}^{\text{ZF}}[m]\|_2}$ . In the denominator,  $\text{MUI}_{d,m} \approx 0$  due to the ZF precoding, when  $N \geq D$ . Furthermore,  $\text{var}\{z_d^{\text{SI}}\}$  and  $\text{var}\{z_d^{\text{IMI}}\}$  can be obtained as follows

$$\begin{aligned} \text{var}\{z_d^{\text{SI}}\} &= \mathbb{E}\left[z_d^{\text{SI}}(z_d^{\text{SI}})^H\right] \stackrel{(a)}{=} \xi_d^{\text{SI}} \sum_{\bar{m} \in \mathcal{M}} p_{d\bar{m}} \\ \text{var}\{z_d^{\text{IMI}}\} &= \xi_d^{\text{IMI}} \mathbb{E}\left[z_d^{\text{IMI}}(z_d^{\text{IMI}})^H\right] \stackrel{(b)}{=} \\ &\xi_d^{\text{IMI}} \sum_{d' \in \mathcal{D} \setminus \{d\}} \sum_{\bar{m} \in \mathcal{M}} \frac{\beta_{dd'}}{M_{\text{sum}}} \bar{m} p_{d'\bar{m}} \end{aligned} \quad (15)$$

where (a) is derived using  $\mathbb{E}[h_{dd}h_{dd}^H] = \xi_d^{\text{SI}}$  according to (1), and (b) is obtained using  $\mathbb{E}[h_{dd'}[m]h_{dd'}^H[\bar{m}]] = \mathbb{E}[(\boldsymbol{\phi}_{\text{UL}}^T \mathbf{F} \boldsymbol{\Psi} \mathbf{g}_{dd'}) (\boldsymbol{\phi}_{\text{UL}}^T \mathbf{F} \boldsymbol{\Psi} \mathbf{g}_{dd'})^H] = \frac{\beta_{dd'}}{M_{\text{sum}}}$ .

For the  $\text{SINR}_{d,\bar{m}}$ , since  $(\mathbf{w}_{ld}^{\text{ZF}}[\bar{m}])^H \mathbf{h}_{ld}^{\text{ZF}}[\bar{m}] \approx 1$ , the term in the numerator of (6) can be changed to  $p_{d\bar{m}} L^2$ . In the denominator,  $\text{MUI}_{d,\bar{m}} \approx 0$ , while the second term can be obtained as

$$\begin{aligned} &\sum_{l \in \mathcal{L}} \mathbb{E}\left[\left\|\left(\mathbf{w}_{ld}^{\text{ZF}}[\bar{m}]\right)^H \mathbf{z}_l^{\text{SI}}\right\|^2\right] \\ &= \sum_{l \in \mathcal{L}} \text{Tr}\left[\left(\mathbf{w}_{ld}^{\text{ZF}}[\bar{m}]\right)^H \text{diag}\left(\text{cov}\{z_l^{\text{SI}}\}\right) \mathbf{w}_{ld}^{\text{ZF}}[\bar{m}]\right] \\ &\stackrel{(a)}{=} \xi_l^{\text{SI}} \sum_{l \in \mathcal{L}} \left\|\mathbf{w}_{ld}^{\text{ZF}}[\bar{m}]\right\|_2^2 \sum_{m \in \mathcal{M}} \sum_{d \in \mathcal{D}} p_{ldm} \end{aligned} \quad (16)$$

where (a) is due to

$$\begin{aligned} (\text{cov}\{z_l^{\text{SI}}\})_{i,i} &= \sum_{m \in \mathcal{M}} \sum_{d \in \mathcal{D}} p_{ldm} \mathbb{E}\left[\left|\mathbf{H}_l^{(i,:)} \mathbf{f}_{ld}^{\text{ZF}}[m] x_d[m]\right|^2\right] \\ &\stackrel{(b)}{=} \sum_{m \in \mathcal{M}} \sum_{d \in \mathcal{D}} p_{ldm} \text{Tr}\left[\mathbf{f}_{ld}^{\text{ZF}}[m] \left(\mathbf{f}_{ld}^{\text{ZF}}[m]\right)^H \mathbb{E}\left[\left(\mathbf{H}_l^{(i,:)}\right)^H \mathbf{H}_l^{(i,:)}\right]\right] \\ &\stackrel{(c)}{=} \xi_l^{\text{SI}} \sum_{m \in \mathcal{M}} \sum_{d \in \mathcal{D}} p_{ldm} \end{aligned} \quad (17)$$

where we have (b) since the ZF precoder only considers the desired signal, and hence the ZF precoding vector is uncorrelated with the SI channel, we have (c) according to the as-

sumption that  $\|\mathbf{f}_{ld}^{\text{ZF}}[m]\|_2^2 = 1$  and  $\mathbb{E}\left[\left(\mathbf{H}_l^{(i,:)}\right)^H \mathbf{H}_l^{(i,:)}\right] = \xi_l^{\text{SI}} \mathbf{I}_N$ .

Similarly, the third term in the denominator of (6) can be obtained as

$$\begin{aligned} &\sum_{l \in \mathcal{L}} \mathbb{E}\left[\left\|\mathbf{w}_{ld}^H[\bar{m}] \mathbf{z}_l^{\text{IAI}}\right\|^2\right] \\ &= \xi_l^{\text{IAI}} \sum_{l \in \mathcal{L}} v_{ld\bar{m}} \sum_{l' \in \mathcal{L} \setminus \{l\}} \sum_{m \in \mathcal{M}} \sum_{d \in \mathcal{D}} \frac{\beta_{ll'}}{M_{\text{sum}}} p_{l'dm} \end{aligned} \quad (18)$$

where  $v_{ld\bar{m}} = \left\|\mathbf{w}_{ld}^{\text{ZF}}[\bar{m}]\right\|_2^2$ . Then, the  $\text{SINR}_{d,m}$  and  $\text{SINR}_{d,\bar{m}}$  can be simplified to the desired form as shown in (7).

## REFERENCES

- [1] Ö. T. Demir, E. Björnson, and L. Sanguinetti, "Foundations of user-centric cell-free massive MIMO," *arXiv preprint arXiv:2108.02541*, 2021.
- [2] S. Goyal, P. Liu, S. S. Panwar, R. A. Difazio, R. Yang, and E. Bala, "Full duplex cellular systems: will doubling interference prevent doubling capacity?" *IEEE Communications Magazine*, vol. 53, no. 5, pp. 121–127, 2015.
- [3] S. Elhoushy, M. Ibrahim, and W. Hamouda, "Cell-free massive mimo: A survey," *IEEE Communications Surveys & Tutorials*, 2021.
- [4] K. E. Kolodziej, B. T. Perry, and J. S. Herd, "In-band full-duplex technology: Techniques and systems survey," *IEEE Transactions on Microwave Theory and Techniques*, vol. 67, no. 7, pp. 3025–3041, 2019.
- [5] E. Everett, A. Sahai, and A. Sabharwal, "Passive self-interference suppression for full-duplex infrastructure nodes," *IEEE Transactions on Wireless Communications*, vol. 13, no. 2, pp. 680–694, 2014.
- [6] X. Quan, Y. Liu, W. Pan, Y. Tang, and K. Kang, "A two-stage analog cancellation architecture for self-interference suppression in full-duplex communications," in *2017 IEEE MTT-S International Microwave Symposium (IMS)*. IEEE, 2017, pp. 1169–1172.
- [7] E. Ahmed and A. M. Eltawil, "All-digital self-interference cancellation technique for full-duplex systems," *IEEE Transactions on Wireless Communications*, vol. 14, no. 7, pp. 3519–3532, 2015.
- [8] D. Liang, P. Xiao, G. Chen, M. Ghorraishi, and R. Tafazolli, "Digital self-interference cancellation for full-duplex mimo systems," in *2015 International Wireless Communications and Mobile Computing Conference (IWCMC)*. IEEE, 2015, pp. 403–407.
- [9] M. Ghorraishi, W. Jiang, P. Xiao, and R. Tafazolli, "Subband approach for wideband self-interference cancellation in full-duplex transceiver," in *2015 International Wireless Communications and Mobile Computing Conference (IWCMC)*. IEEE, 2015, pp. 1139–1143.
- [10] B. Li, L.-L. Yang, R. G. Maunder, P. Xiao, and S. Sun, "Multicarrier-division duplex: A duplexing technique for the shift to 6g wireless communications," *IEEE Vehicular Technology Magazine*, 2021.
- [11] J. M. B. da Silva, G. Wikström, R. K. Mungara, and C. Fischione, "Full duplex and dynamic TDD: Pushing the limits of spectrum reuse in multi-cell communications," *IEEE Wireless Communications*, vol. 28, no. 1, pp. 44–50, 2021.
- [12] H. Kim, J. Kim, and D. Hong, "Dynamic TDD systems for 5G and beyond: A survey of cross-link interference mitigation," *IEEE Communications Surveys & Tutorials*, vol. 22, no. 4, pp. 2315–2348, 2020.
- [13] H. V. Nguyen, V.-D. Nguyen, O. A. Dobre, S. K. Sharma, S. Chatzinotas, B. Ottersten, and O.-S. Shin, "On the spectral and energy efficiencies of full-duplex cell-free massive MIMO," *IEEE Journal on Selected Areas in Communications*, vol. 38, no. 8, pp. 1698–1718, 2020.

- [14] X. Xia, P. Zhu, J. Li, H. Wu, D. Wang, Y. Xin, and X. You, "Joint user selection and transceiver design for cell-free with network-assisted full duplexing," *IEEE Transactions on Wireless Communications*, 2021.
- [15] D. Wang, M. Wang, P. Zhu, J. Li, J. Wang, and X. You, "Performance of network-assisted full-duplex for cell-free massive MIMO," *IEEE Transactions on Communications*, vol. 68, no. 3, pp. 1464–1478, 2019.
- [16] L. You, Y. Huang, D. Zhang, Z. Chang, W. Wang, and X. Gao, "Energy efficiency optimization for multi-cell massive mimo: Centralized and distributed power allocation algorithms," *IEEE Transactions on Communications*, vol. 69, no. 8, pp. 5228–5242, 2021.
- [17] K. Shen and W. Yu, "Fractional programming for communication systems—part I: Power control and beamforming," *IEEE Transactions on Signal Processing*, vol. 66, no. 10, pp. 2616–2630, 2018.
- [18] D. N. Amudala, E. Sharma, and R. Budhiraja, "Spectral efficiency optimization of spatially-correlated multi-pair full-duplex massive mimo relaying," *IEEE Transactions on Communications*, vol. 67, no. 12, pp. 8346–8364, 2019.
- [19] F. Fang, Z. Ding, W. Liang, and H. Zhang, "Optimal energy efficient power allocation with user fairness for uplink mc-noma systems," *IEEE Wireless Communications Letters*, vol. 8, no. 4, pp. 1133–1136, 2019.
- [20] J.-W. Li and C. Lin, "On the optimal power allocation for two-way full-duplex af relay networks," *IEEE Transactions on Signal Processing*, vol. 65, no. 21, pp. 5702–5715, 2017.
- [21] X. Xu, X. Chen, M. Zhao, S. Zhou, C.-Y. Chi, and J. Wang, "Power-efficient distributed beamforming for full-duplex mimo relaying networks," *IEEE Transactions on Vehicular Technology*, vol. 66, no. 2, pp. 1087–1103, 2016.
- [22] W. Lee, M. Kim, and D.-H. Cho, "Deep power control: Transmit power control scheme based on convolutional neural network," *IEEE Communications Letters*, vol. 22, no. 6, pp. 1276–1279, 2018.
- [23] F. Liang, C. Shen, W. Yu, and F. Wu, "Towards optimal power control via ensembling deep neural networks," *IEEE Transactions on Communications*, vol. 68, no. 3, pp. 1760–1776, 2019.
- [24] L. Luo, J. Zhang, S. Chen, X. Zhang, B. Ai, and D. W. K. Ng, "Downlink power control for cell-free massive mimo with deep reinforcement learning," *IEEE Transactions on Vehicular Technology*, 2022.
- [25] Y. Zhao, I. G. Niemegeers, and S. M. H. De Groot, "Dynamic power allocation for cell-free massive mimo: Deep reinforcement learning methods," *IEEE Access*, vol. 9, pp. 102 953–102 965, 2021.
- [26] M. Bashar, A. Akbari, K. Cumanan, H. Q. Ngo, A. G. Burr, P. Xiao, and M. Debbah, "Deep learning-aided finite-capacity fronthaul cell-free massive mimo with zero forcing," in *ICC 2020-2020 IEEE International Conference on Communications (ICC)*. IEEE, 2020, pp. 1–6.
- [27] M. Zaher, Ö. T. Demir, E. Björnson, and M. Petrova, "Learning-based downlink power allocation in cell-free massive mimo systems," *arXiv preprint arXiv:2109.03128*, 2021.
- [28] Y. Shen, Y. Shi, J. Zhang, and K. B. Letaief, "Graph neural networks for scalable radio resource management: Architecture design and theoretical analysis," *IEEE Journal on Selected Areas in Communications*, vol. 39, no. 1, pp. 101–115, 2020.
- [29] A. Chowdhury, G. Verma, C. Rao, A. Swami, and S. Segarra, "Unfolding wmmse using graph neural networks for efficient power allocation," *IEEE Transactions on Wireless Communications*, vol. 20, no. 9, pp. 6004–6017, 2021.
- [30] M. Eisen and A. Ribeiro, "Optimal wireless resource allocation with random edge graph neural networks," *IEEE transactions on signal processing*, vol. 68, pp. 2977–2991, 2020.
- [31] B. Li, L.-L. Yang, R. G. Maunder, and S. Sun, "Self-interference cancellation and channel estimation in multicarrier-division duplex systems with hybrid beamforming," *IEEE Access*, vol. 8, pp. 160 653–160 669, 2020.
- [32] B. P. Day, A. R. Margetts, D. W. Bliss, and P. Schniter, "Full-duplex MIMO relaying: Achievable rates under limited dynamic range," *IEEE Journal on Selected Areas in Communications*, vol. 30, no. 8, pp. 1541–1553, 2012.
- [33] D. W. K. Ng, Y. Wu, and R. Schober, "Power efficient resource allocation for full-duplex radio distributed antenna networks," *IEEE Transactions on Wireless Communications*, vol. 15, no. 4, pp. 2896–2911, 2016.
- [34] Y. Jiang, M. K. Varanasi, and J. Li, "Performance analysis of ZF and MMSE equalizers for MIMO systems: An in-depth study of the high SNR regime," *IEEE Transactions on Information Theory*, vol. 57, no. 4, pp. 2008–2026, 2011.
- [35] Y. Sun and J. Han, "Mining heterogeneous information networks: a structural analysis approach," *Acm Sigkdd Explorations Newsletter*, vol. 14, no. 2, pp. 20–28, 2013.
- [36] X. Wang, H. Ji, C. Shi, B. Wang, Y. Ye, P. Cui, and P. S. Yu, "Heterogeneous graph attention network," in *The world wide web conference*, 2019, pp. 2022–2032.
- [37] W. Cui, K. Shen, and W. Yu, "Spatial deep learning for wireless scheduling," *IEEE journal on selected areas in communications*, vol. 37, no. 6, pp. 1248–1261, 2019.
- [38] M. Fey and J. E. Lenssen, "Fast graph representation learning with pytorch geometric," *arXiv preprint arXiv:1903.02428*, 2019.
- [39] D. P. Kingma and J. Ba, "Adam: A method for stochastic optimization," *arXiv preprint arXiv:1412.6980*, 2014.
- [40] M. Grant and S. Boyd, "CVX: Matlab software for disciplined convex programming, version 2.1," <http://cvxr.com/cvx>, Mar. 2014.
- [41] J. Jang and K. B. Lee, "Transmit power adaptation for multiuser OFDM systems," *IEEE Journal on selected areas in communications*, vol. 21, no. 2, pp. 171–178, 2003.
- [42] D. Peaucelle, D. Henrion, Y. Labit, and K. Taitz, "User's guide for sedumi interface 1.04," *LAAS-CNRS, Toulouse*, 2002.